On the structure of cumulus clouds

by

S J Caughey

Introduction:

This lecture summarises some recent findings concerning the dynamical and microphysical structures of cumulus clouds. It is perhaps surprising that at present the available information is quite sparse (so that various interpretations are possible) and the subject is still one of some controversy. However, there are severe difficulties associated with making detailed and precise observations of a rapidly changing and complex phenomenon such as cumulus convection and this, to some extent, explains the lack of progress.

Cumulus clouds generally form near the top of the convective boundary layer (CBL) and may be largely constrained within this layer (cumulus humilis) or develop into major storm clouds and affect atmospheric structure over tens or hundreds of kilometers. This talk is concerned with small to medium sized cumulus i.e. ranging from a few hundred metres to several kilometers in depth. The main observed features of cumulus convection are first described followed by a summary of recent attempts to model the process.

Observational studies

There is no entirely satisfactory method for monitoring the thermodynamical, dynamical and microphysical structures of cumulus clouds which follow an evolutionary sequence which may last from minutes to hours and may or may not include the precipitation stage. Aircraft sampling has the advantage that individual clouds can be tracked and sampled at different stages in the evolutionary cycle but clearly to monitor the vertical structure requires repeated passes at different levels, which may take tens of minutes to complete. Furthermore, large aircraft (such as the C130 available to the UK Met Office) disturb the cloud and this introduces uncertainty into the measurements. Multilevel fixed point sampling (eg from a tethered balloon) overcomes these disadvantages to some degree but generally provides only a short sample in the lifetime of a particular cloud. Clearly to build up a comprehensive description of cumulus structure requires information from both sampling techniques.

It is also necessary to record the entire range of relevant parameters eg the details of the cloud droplet field and air motion (down to small scales) etc, to gain some appreciation for the interaction of the turbulent cloud with the (generally) non-turbulent environment. Early studies of cumulus concentrated on specifying details of the droplet field without due regard for the dynamical framework within which this was set (see eg Zaitsev (1950), Squires (1958) and Durbin (1959)).

During the 1960's Warner (1969) made a series of aircraft observations of cumulus of depth 1-5 km whose tops were warmer than $-10^{\circ}C$. These clouds generally formed in maritime air and hence condensation nuclei concentrations (CCN) were probably low. These data remain the most comprehensive available on most aspects of cumulus structure. Shown in Fig 1(a) are the observed droplet size distributions with height in a typical cloud. Some noteworthy aspects are the increase in width of the spectrum with height above cloud base and the suggestion of a bi-modal spectral shape near cloud top. Other transits near cloud top showed a quite

pronounced bimodal shape (Fig 1(b)). Warner investigated the variation of the fraction of bimodal distributions with environmental lapse rate and found a strong decrease with increasing stability ie when $\partial T/\partial z$ (environment) exceeded 6–7°C/km then no bimodal spectra were found. Since the stability of the surrounding air is a factor influencing the entrainment of air into cloud Warner took this result to indicate that bimodal spectra were somehow generated by mixing between cloud and environment.

Squires (1958) remarked that, "the droplet spectrum has been found to change rapidly and erratically in all clouds sampled". Warner's observations, to some degree, supported this but also demonstrated consistency between samples at 100 m intervals, for eg Fig 1(c), which shows correspondence between bimodal spectra sampled within a region of strong updraft and high liquid water content.

Early studies indicated no significant variation in the total droplet concentration with height and this was supported by Warner's data (see Fig 2(a)). This suggests that the growth in droplet size with height (Fig 2(b)) must be accounted for by condensation rather than by coalescence. Twomey (1966) suggested that as clouds formed the initial coefficient of dispersion ($\sigma = \frac{\text{standard deviation}}{\text{mean size}}$) is ~ 0.2. In agreement with this Warner found σ to increase from about this value near cloud base to reach $\sim .45$ at $1\frac{1}{2}$–2 km above the base (Fig 2(c)).

In some later studies Warner (1973) investigated the variation of some microphysical characteristics with time, which is clearly important in assessing the significance of observations made at some arbitrary point in the lifetime of an individual cloud. It is not, of course, possible to follow a particular parcel of cloudy air, however it is not even clear how the droplet spectrum, at a particular level in a cloud, changes with time. In fact Warner observed comparatively little change in the droplet spectral shape from traverse to traverse (Fig 2(d)), which remained a characteristic of the cloud sampled. Other parameters such as the mean droplet diameter and dispersion consequently also showed little variation with time (Fig 3(a) and (b)). It is important to note, however, that these remarks apply only to the cloud droplet spectrum and not of course to the development of hydrometeors at the 'tail' of the size distribution. There was some evidence (Fig 3(c)) that droplet concentration initially increased with time and then decreased as the clouds aged and began to dissipate.

In carrying out these studies Warner made some attempts at monitoring and interpreting the vertical air motion in cumulus. Whilst earlier studies specified in fair detail the microphysical structure Warner noted that little information existed on the nature of the updraft or the mixing between clouds and their environment. As a result of his observations (see Warner (1969)) he drew three main conclusions on the character of the vertical velocity field, which exhibited,

(a) a chaotic structure near cloud base not necessarily bearing much relationship to the cloud liquid water.

(b) a general updraft region in the body of the cloud which in its broader features often parallels the liquid water variations.

(c) a strongly turbulent region near cloud top which again parallels the liquid water in its broader features but often exhibits strong downdrafts.

Warner produced horizontal gust vector plots to examine air motion along the flight path (see Figure (4)). From these and similar data he concluded that only traverses near cloud top showed evidence for organised overturning motions. Similar results

have been obtained from aircraft in Colarado cumuli 1–4½ km deep by MacPherson and Isaacs (1977) and in small fair-weather cumulus over land in the UK by Kitchen and Caughey (1981). These latter results were obtained from tethered balloon-borne turbulence probes and represent the first simultaneous multilevel observations in cumulus. A striking feature of the data in the marked vertical coherence of the updraft and the occurance of strong downdrafts near cloud top (see Fig (5)). Presenting the data in gust vector form provides some evidence for rotation near cloud top (as suggested by Warner's data) so that the overall circulation assumes a characteristic 'P' shape (Fig (6)). Bennetts and Gloster (1980) have recently shown how 'P' type circulations may lead to the development of bimodal droplet spectra.

In the studies conducted by Warner the peak updrafts and downdrafts were found to increase with height above cloud base (Fig 7(a)) as did the standard deviation of the vertical velocity fluctuations (σ_w). The σ_w variation was well fitted by the regression

$$\sigma_w \sim 1.26 + 0.76 z$$

where σ_w is averaged over the cloud width.

To examine the vertical velocity field for preferred or 'characteristic' scales of motion it is useful to compute the spectral distribution of the fluctuations (by taking the Fourier transform of the time history). Some examples of vertical velocity power spectra obtained by Warner are given in Fig 7(b). Part (i) shows the average spectrum for three runs within 300m of cloud base and for three runs within 300m of cloud top. In Part (ii) the mean of these two spectra is compared with the average spectra for runs 300–600m and 600–900m from either base or top (whichever is the closer). These spectra suggest that most of the energy is concentrated at the long wavelength end of the spectrum (wavelengths of a few kilometers) but there is also a considerable amount of energy present near cloud base and top in wavelengths between 100–200m. There is little doubt that the long wavelengths are generated as a result of the release of latent heat over a large fraction of the cloud width and thus reflect the main updraft structure. The shorter wavelengths are due to the associated turbulence field and, especially near cloud top, to mixing processes. It is worth noting that the power spectra obtained by Warner exhibited a slope of −2 at the high frequency end, instead of the $-1\frac{2}{3}$ slope expected from the inertial subrange region of homogeneous isotropic turbulence. This means that these spectra cannot be used to estimate the local rate of dissipation of turbulence kinetic energy, ε.

In some recent studies Kitchen and Caughey (1981) have also found mulitple peaks in power spectra of vertical motion in small cumulus. The lower frequency peak at the cloud top level (Fig (8)) corresponds to a wavelength of $\sim\frac{1}{2}$ km and, as in Warner's data, is generated by motion on the scale of the major up- and downdrafts. The increased spectral density at higher frequencies is due to turbulence and it is significant that the $-1\frac{2}{3}$ slope, characteristic of the inertial subrange only begins at $\sim$ 0.5 H_z (corresponding to a scale of $\sim$10–20m). That the remainder of the spectrum is not inertial is supported by the cospectrum of u (longitudinal) and v (lateral) velocities, which shows that cospectral levels rise rapidly for scales larger than that corresponding to the higher frequency peak. There is some evidence for a shift in both peaks to higher frequency as cloud top is approached, presumably due to the influence of the capping inversion. Clearly spectra from aircraft traverses of cumulus, which have more limited spatial resolution, may yield single peaked spectra of rather variable slope, but since the spectral decay from the first peak is rapid this will generally be $> -1\frac{2}{3}$, as indeed found by Warner.

In any complete investigation of cumulus it is of course necessary to examine the dynamical and microphysical structures simultaneously, in order to properly interpret the data. So far this has not been achieved in an entirely satisfactory way. Some results from Kitchen and Caughey (1981) are interesting in this respect (see Fig (9)). This shows cloud data from a turbulence probe at 1325 m and a droplet spectrometer which passed through the top of the cumulus. Liquid water contents in this region averaged $\sim \frac{1}{2}$ the adiabatic value. The most striking feature of the data is the insensitivity of either the mean droplet radius or dispersion to extreme variations in droplet concentration. This strongly suggests an inhomogenous cloud structure in which certain regions have been largely depleted of droplets. An examination of droplet spectra from high ($> .075$ g m^{-3}) and low ($< .025$ g m^{-3}) liquid water content regions confirms this view (see Fig (10)), with only small changes in spectral shape introduced during evaporation, a feature characteristic of the laboratory studies of Latham and Reed (1977). This topic is discussed further in the next section.

Theoretical Aspects

The foregoing studies indicate a need for a treatment of cloud microphysics within some realistic dynamical framework. This should include microphysical effects produced by mean flow considerations such as the 'P' type circulations discussed earlier together with entrainment and mixing of environmental air with cloudy air on a range of scales. Thus far theoretical treatments have fallen short of this ideal, however the current appreciation for the importance of dynamical effects may result in real progress soon being made.

There are four principal aspects of the microphysics that require explanations

(i) droplets of the smallest detectable size (dia $\sim$ 5 μm) are found at all levels within clouds

(ii) the droplet spectrum is consequently broad and is commonly found to be bimodal

(iii) the dispersion of the spectrum is $\sim$ 0.2 near cloud base and increases with height

(iv) related to the above points is that the measured times required to produce raindrops in water clouds may be appreciably shorter than the values calculated on the classical theory of droplet growth followed by coalescence.

Mason and Chien (1962) noted that condensation on a realistic spectrum of soluble nuclei in an ascending air parcel cooling adiabatically without mixing with its surroundings produces much narrower droplet spectra than are actually observed and cannot account for high concentrations of small droplets ($\sim$ 5 μm dia) because theory predicts that all these should have exceeded this size $\sim$ 100 m above cloud base. Moreover such simple models cannot account for bimodal spectra nor the production of droplets $> \sim$ 20 μm.

The fact that clouds, and more particularly the updraft regions, are turbulent was considered by Bartlett and Jonas (1972) who supposed that neglect of this might be responsible for the discrepancies between the observed and calculated dispersions. An earlier study by Warner (1969) led him to conclude that, in general "turbulence in the updraft does not broaden the droplet size distribution markedly beyond that produced by condensation in a steady updraft". The treatment by Bartlett and Jonas

was more thorough and involved solving a set of equations for the changes in temperature, supersaturation, liquid water content in an adiabatically ascending parcel of air. In doing this it was not assumed that the air is always just saturated but instead the equation for the rate of growth of droplets at a given supersaturation is used to determine the rate of transfer of water substance from the vapour to the liquid phase. This set of simultaneous differential equations was solved numerically and the vertical velocity of the parcel was specified at each step of the integration by simulation with a random number generator. The mean updraft velocity was set at ~ 1 ms^{-1}. Fig 11(a) shows the fluctuating velocity time history of a particular parcel and also shows the way in which the supersaturation varies. It is apparent that these are quite closely correlated, although the supersaturation lags vertical velocity by ~ 5 s and the highest frequencies are damped out. Typical droplet trajectories are shown in Fig 11(b). In 'A' a droplet ascends (apart from a small downwards excursion), in 'B' the particle initially descends and then rises whereas in 'C' the particle descends and eventually evaporates. Calculations were performed a large number of times following particles to 3 km above the starting level. These simulations showed an extremely small spread in the droplet sizes at any particular level in the cloud (see Table1). Even very turbulent clouds produced only a little spread. These results therefore supported Warner's earlier conclusion in that turbulent fluctuations in updrafts do not produce a significant spread in drop sizes. This arises because the supersaturations and updrafts which a growing drop encounters are closely correlated, hence a droplet which experiences a high supersaturation and therefore grows rapidly is likely to be in a strong updraft which will allow it only a relatively short time to grow in passing between any 2 levels in the clouds. Conversely low supersaturations are associated with small updrafts and long growth times.

In an attempt to explore the effects of mixing within a simple dynamical framework Mason and Jonas (1974) extended the computations of Mason and Chien (1962), which dealt with only a single rising thermal, to study the effect on the evolution of droplet spectra of allowing the thermal, after reaching its maximum height, to sink back as a result of evaporative cooling (following dry air entrainment) and then to become mixed with a second thermal rising through it. The model input parameters were the initial radius of the thermal (R_o), vertical velocity (U_o), temperature excess, (T-T') of the thermal at the condensation level, the lapse rate, humidity of the environment and initial condensation nucleus spectrum. Mixing between the cloud and environment was parameterised using the equation

$$\frac{1}{M}\frac{dM}{dt} = \frac{\mu U}{R}$$

where M is the mass of the thermal and μ is the mixing parameter. (See Table 2).

The main results were confined to only two examples, one intended to typify a small maritime cumulus containing a low concentration of nuclei/drops and the other being representative of a continental cloud containing a much higher proportion of drops. For the maritime cloud Fig 12(a) shows that the centre of the first thermal, crossing the condensation level with an initial radius of 350m, velocity ~ 1 ms^{-1} and temperature excess of 0.1 deg C attains a maximum height of 0.33 km before coming to rest. The maximum vertical velocity is only 1.01 ms^{-1} at a height of $\sim$ 30 m and the maximum liquid water content is 0.39/kg or $\sim \frac{1}{3}$ of the adiabatic value. On attaining the level of zero buoyancy the thermal now mixes with the surrounding air of 85% humidity, the progress of its evaporation and descent being depicted in Fig 12(b). A new thermal is now assumed to cross the condensation level with the same properties as its predecessor, but it now mixes with the residue of the old thermal assumed to be quiescent and just saturated. On emerging from the old thermal it continues to mix with the drier environmental air, soon reaches a maximum velocity of 1.6 km, a maximum radius of 670 m , the total time elapsed being 35 minutes (Fig 12(c)). Over the upper $\frac{3}{3}$ of the ascent liquid water contents range from

0.6 g/kg to 0.9 g/kg or about 0.35 of the adiabatic value and supersaturations reach a peak value of 0.4%.

Computed spectra for the region near cloud base and 1400 m above it are shown by the histograms in Figure 13(a) and (b), while the dashed lines indicate the spectra obtained by Warner at these levels in a cloud of similar size. The general agreement between the computed and observed spectra is fair, the observed bimodality with a second peak at 15-20 μm being well predicted.

The development of a continental cloud growing under the same environmental conditions and starting with the same initial radius and vertical velocity, but with a temperature excess of 0.6 deg C and total nucleus population of 530/mg of air is given in Fig (14). The evolution of the droplet spectrum in the model continental cloud showed that, even in the last stages of ascent of a second thermal, the largest drops do not exceed 20 μm in radius and the concentration of 19-20 μm droplets is only 30 m^{-3}. A bimodal shape also appeared but was less marked than for the maritime cloud.

Mason and Jonas claimed that their model appeared to have solved the long-standing problem of how to account for the production by condensation of droplets of $\sim$ 25μm radius in concentrations of $\sim$ 100 m^{-3} in a reasonably short time ($\sim \frac{1}{2}$ hr). Their paper was, however, criticised by Warner (1975) and defended by Mason (1975). In essence Warner objected to the simple dynamical framework employed and also believed that the thermodynamics of the mixing was poorly treated.

In a further paper Jonas and Mason (1974) described the results of calculations to investigate the development of droplet spectra by condensation and coalescence in a rising thermal from the instant that it emerges from an earlier decayed thermal into the clear air above. Up to this time the drops are assumed to have grown solely by condensation as in Mason and Jonas (1974). The further development of the previously discussed maritime cloud is shown in Fig 15(a). The spectrum broadens quite rapidly and by the time it reaches its maximum level of 1.6 km drops of radius $\sim$100 μm appear in concentrations of $\sim$ 100/m^3. For the continental case the spectrum broadens only slowly and after 15 mins, by which time the cloud has reached a maximum level of 1.6 km, no droplets have exceeded 25 μm radius.

Although the larger drops grow predominantly by coalescence continued growth by condensation has a marked effect in that it enhances the growth rates of smaller drops which are then captured more efficiently by the larger ones. Figure 15(b) compares the development of an initial spectrum over a period of 4 mins by coalescence acting alone and when condensation and entrainment are included. Coalescence acting alone produces droplets of only 29 μm radius in concentrations of $\sim$ 100/m^3 after 4 mins and 75 μm after 10 mins. The corresponding droplet radii being 54 μm and 105 μm if condensation and entrainment processes are included.

Although the calculations of Mason and Jonas (1974) have shown that mixing between the cloud and its environment is important there is as yet no widely accepted treatment of this topic. Furthermore it should be noted that in these and similar calculations eg Warner (1973) and Lee and Pruppacher (1977) the mixing process is assumed to be homogeneous. In other words, all droplets at a given level in the cloud are, at any time, exposed to the identical conditions of supersaturation or under-saturation. Laboratory studies by Latham and Reed (1977), in which spectral changes were examined as undersaturated air was entrained into a slowly moving population of cloud droplets, yielded an alternative description of the mixing process. It is that the intermingling of cloudy and environmental air is a highly inhomogeneous process, with those droplets immediately adjacent to infiltrating filaments or blobs of undersaturated air being drastically affected, while those more remote being less so, or even unaffected. Subsequent mixing will produce a broad spectrum. This process appears to have three favourable attributes,

(1) it associates the major spectral properties with a single process - entrainment, which is known to be important.

(2) it provides a mechanism for producing inhomogeneities in supersaturation which are not intimately tied to changes in updraft speed - thus circumventing the major obstacle to spectral broadening isolated by Bartlett and Jonas (1972) and

(3) it provides a mechanism for the more rapid growth by diffusion of some fraction of the droplets in the condensate spectrum.

In a recent paper Baker et al (1980) have elaborated somewhat on the concept of inhomogeneous mixing. They suggest that the extent to which this process may be applicable in particular circumstances depends upon certain rate processes associated with the mixing process in clouds. These are turbulent diffusion of the entrained air into the cloud; molecular diffusion at the interface between a blob and the surrounding cloudy air and the evaporation of droplets in an undersaturated environment. The characteristic times governing these three processes are defined as τ_T, τ_D and τ_r respectively. If τ_T or τ_D are much less than τ_r any inhomogeneities created by the mixing process will be substantially smoothed out before significant droplet evaporation can occur and the mixing will approach the classical description employed by other workers. However if the reverse is true then the mixing will approximate the inhomogeneous description.

Taking X as the characteristic size of the entrained air parcel, ε the rate of kinetic energy dissipation via turbulent mixing, D the molecular diffusion coefficient, S(%) the supersaturation, α ($\sim 5\ \mu$m) the length scale associated with the condensation coefficient we may write,

$$\tau_T \sim (X^2/\varepsilon)^{1/3}$$

$$\tau_D \sim (X^2/D)$$

$$\tau_r \sim 10^{-6}\left(\frac{\rho_w}{\rho_\infty}\right)\left[(r+\alpha)^2-\alpha^2\right]/DS$$

Where r is in micrometres and ρ_w/ρ_∞ ($\sim 10^5$) is the ratio of the densities of liquid water and saturated vapour. Assuming $\varepsilon \sim 100$ cm^2 sec^{-3}, D ~ 0.25 cm^2 sec^{-1} we find that $\tau_T \ll \tau_D$ for all scales of interest. Thus the nature of the mixing will depend upon the relative values of τ_T and τ_r. Table (3) presents values of the length scale X_c (= $\varepsilon^{1/2}\tau_r^{3/2}$) for which $\tau_T/\tau_r = 1$ for various values of r, S and ε. It is seen that except for the highest levels of turbulence combined with low undersaturations the evaporation may be non-classical for scales in excess of about one metre.

In order to examine the influence on droplet spectral evolution of the inhomogeneous mixing of undersaturated and cloudy air Baker et al, modelled a simple mechanism which represents an extreme, or limiting, case corresponding to the condition $\tau_r/\tau_T \rightarrow 0$. In this model parcels of volume v_o and relative humidity H are entrained into an ascending parcel of cloud, of volume V, at a constant mean rate $\lambda(t)$.

A comparison of the predictions of their simple inhomogeneous model with the observations of Warner (1969) is provided in Figure (16)a and b. The agreement between the observed and inhomogeneous spectra is very good in both cases -

deviations at the smaller droplet size possibly being due to experimental difficulty in sampling droplets of r ~ 2 μm with a sooted-slide technique as well as the crudeness of the model. On the other hand curves (H) based on the homogeneous description of entrainment bear little resemblance to those observed. It was also found that the value of spectral dispersion calculated on the inhomogeneous model increased with height above cloud base and were similar to those observed by Warner. The occurrence of bimodal spectra is also reproduced by the inhomogeneous model when the frequency of infiltration of the clouds by 'blobs' is low. Those generated also strongly resemble the ones observed by Warner (1969).

Concluding remarks

Further advances in the physics of cummulus clouds can be expected to follow the wide introduction of remote particle sensing instrumentation such as Knollenberg's axially scattering spectrometer probe (1970). These instruments provide large quantities of data that are amenable to computer processing and have now largely replaced impactors and coated slides. They should enable comprehensive and wide ranging studies of large and small scale cloud systems.

The concept of inhomogeneous mixing is an intuitively attractive one and merits much more detailed study. There is a need to model, in a realistic manner, the entrainment of a parcel of environment air into a turbulent cloud. In a more general sense there is also a requirement to specify the typical circulations that occur within cummulus, such as the 'P' type mentioned earlier and to investigate the microphysical consequences arising from these. Telford and Chai (1980) have shown that a combination of mixing at cloud top and recycling within cloud can appreciably broaden droplet spectra. Such calculations can be expected to become more realistic as comprehensive measurements of cloud dynamics became available.

List of Figure Captions

Fig 5 Temperature contours (intervals of 0.5°C) from data at the three probe levels (marked — · — · —·). Positions of clouds are indicated by stipling. Below are the vertical velocity traces from the three probes.

Fig 6 Five second gust vectors in the vertical (a) and horizontal (b) planes. A suggested flow pattern is marked (— · — · —·) and cloud boundaries are indicated.

Fig 8 Power spectra of vertical velocity fluctuations,

(a) below cloud base
(b) near cloud top
(c) cospectrum (UW).

Fig 9 Cloud position, temperature contours and vertical velocity at 1173m. Below are mean droplet radius, droplet concentration, liquid water content and dispersion.

Fig 10 Mean droplet spectra for regions of high ($>$ .075 g m^{-3}) and low ($<$ .025 g m^{-3}) liquid water content.

List of References

1. Zaitsev, V.A. 1950 Gla. Geofiz. Obs. Tr. 19, 122-132.

2. Squires, P. 1958 Tellus, 10, 256-271.

3. Durbin, W.G. 1959 Tellus, 11, 202-215.

4. Warner, J. 1969 J. Atmos. Sci., 26, 1049-1059.

5. Twomey, S. 1966 J. Atmos. Sci., 23, 405-411.

6. Warner, J. 1973 J. Atmos. Sci., 30, 1724-1726.

7. MacPherson, J.I. and Isaacs, G.A. 1977 J. App. Met., 16, 81-90.

8. Kitchen, M. and Caughey, S.J. 1981 To appear in Q.J. Roy. Met. Soc.

9. Bennetts, D.A. and Gloster, J. 1980 Proc. VIII International Conference on Cloud Physics, Clermont-Ferrand.

10. Latham, J. and Reed, R.L. 1977 Q.J. Roy. Met. Soc., 103, 297-306.

11. Mason, B.J. and Chien 1962 Q.J. Roy. Met. Soc., 88, 136-142.

12. Bartlett, J.T. and Jonas, P.R. 1972 Q.J. Roy. Met. Soc., 98, 150-164.

13. Warner, J. 1969 J. Atmos. Sci., 26, 1272-1282.

14. Mason, B.J. and Jonas, P.R. 1974 Q.J. Roy. Met. Soc., 100, 23-38.

15. Warner, J. 1975 Q.J. Roy. Met. Soc., 101, 176-178.

16. Mason, B.J. 1975 Q.J. Roy. Met. Soc., 101, 178-188.

17. Jonas and Mason 1974 Q.J. Roy. Met. Soc., 100, 286-295.

18. Lee, I.Y. and Pruppacher, H.R. 1977 Pageoph., 115, 523-545.

19. Baker, M., Corbin, R.G., and Latham, J. 1980 Q.J. Roy. Met. Soc., 106, 581-598.

20. Telford, J.W. and Chai, S.K. 1980 Pageoph., 118, 720-742.

21. Knollenberg, R.G. 1970 J. Appl. Met., 9, 86-103.

TABLE 1 VARIATION IN DROPLET RADIUS WITH HEIGHT IN CLOUD ($E = 0{\cdot}01\ m^2\ s^{-3}$)

Height above starting level (m)	Mean droplet radius (μm)	Standard deviation (μm)
0	5·00	0·00
300	11·39	0·26
600	14·05	0·13
1,200	17·40	0·09
1,800	19·67	0·06
2,400	21·39	0·01
3,000	22·75	0·01

TABLE 2 INITIAL AND PRESCRIBED PARAMETERS FOR CLOUD MODELS (MASON & JONAS 1974).

Temperature and pressure at condensation level		10°C, 900 mb
Initial radius of thermal	R_0	350 m
Initial vertical velocity of thermal	U_0	1·0 m s^{-1}
Initial excess temperature	ΔT_0	0·1°C (maritime), 0·6°C (continental)
Lapse rate of environment	α	7°C km^{-1}
Humidity of environment	H′	85 per cent
Mixing parameter	μ	0·6

Mass of nuclei (g of NaCl)		5×10^{-16}	10^{-15}	3×10^{-15}	10^{-14}	3×10^{-14}	10^{-13}	3×10^{-13}	10^{-12}	3×10^{-12}	10^{-11}	Total Conc^n.
Concentration	Mar	$3{\cdot}8 \times 10^4$	$1{\cdot}9 \times 10^4$	6×10^3	$1{\cdot}9 \times 10^3$	6×10^2	$1{\cdot}9 \times 10^2$	60	19	6	1·9	$6{\cdot}6 \times 10^4$/g.
(per g of air)	Con	$3{\cdot}0 \times 10^5$	$1{\cdot}5 \times 10^5$	$4{\cdot}8 \times 10^4$	$1{\cdot}5 \times 10^4$	$4{\cdot}8 \times 10^3$	$1{\cdot}5 \times 10^3$	480	150	48	15	$5{\cdot}3 \times 10^5$/g.

TABLE 3 VALUES OF THE CRITICAL DISTANCE X_c (cm) PREDICTED FROM EQS. (1) AND (3) FOR VARIOUS VALUES OF DROPLET RADIUS (r), SUPERSATURATION (S) AND RATE OF KINETIC ENERGY DISSIPATION (ε).

	$S = -20\%$			$S = -5\%$		
r (μm)	$\varepsilon = 1$ (cm^2 s^{-3})	$\varepsilon = 10$ (cm^2 s^{-3})	$\varepsilon = 100$ (cm^2 s^{-3})	$\varepsilon = 1$ (cm^2 s^{-3})	$\varepsilon = 10$ (cm^2 s^{-3})	$\varepsilon = 100$ (cm^2 s^{-3})
1	0·1	0·3	1·0	0·8	2·6	8·2
3	0·7	2·1	6·8	5·5	17	55
5	1·8	5·8	18	15	46	147
10	8·0	25	80	64	200	640
15	21	65	210	175	550	1750
20	42	130	420	330	1050	3325

(a)

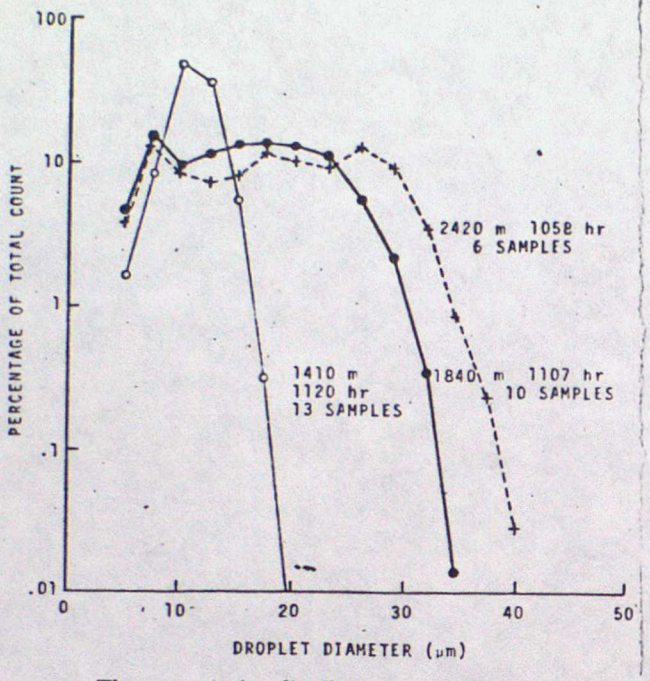

The average size distribution of all samples taken at three different levels in a cloud based at 1220 m and with tops ~2600 m.

(b)

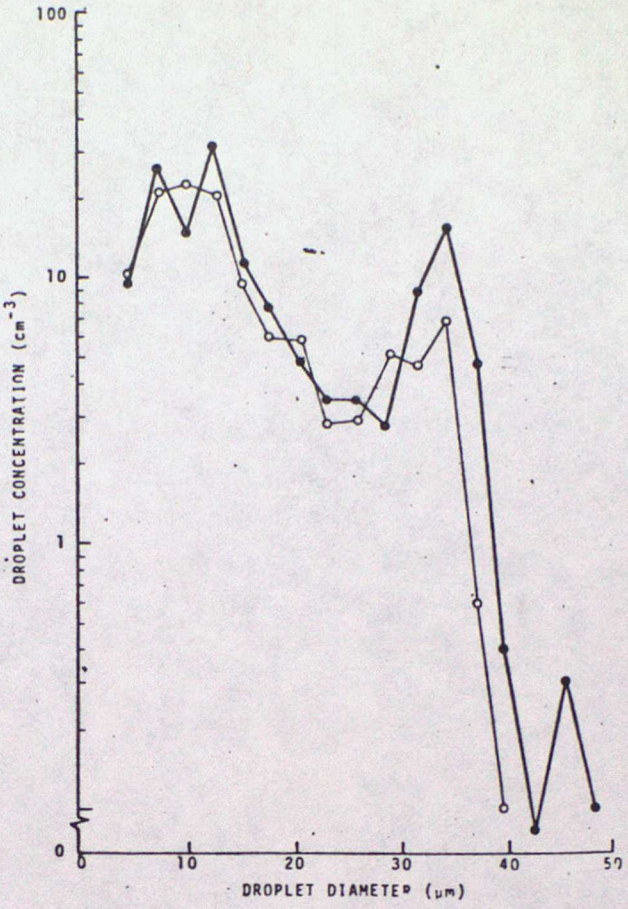

Adjacent samples taken 100 m apart near the top of a cloud 1400 m deep. Both show a strongly bimodal distribution.

(c)

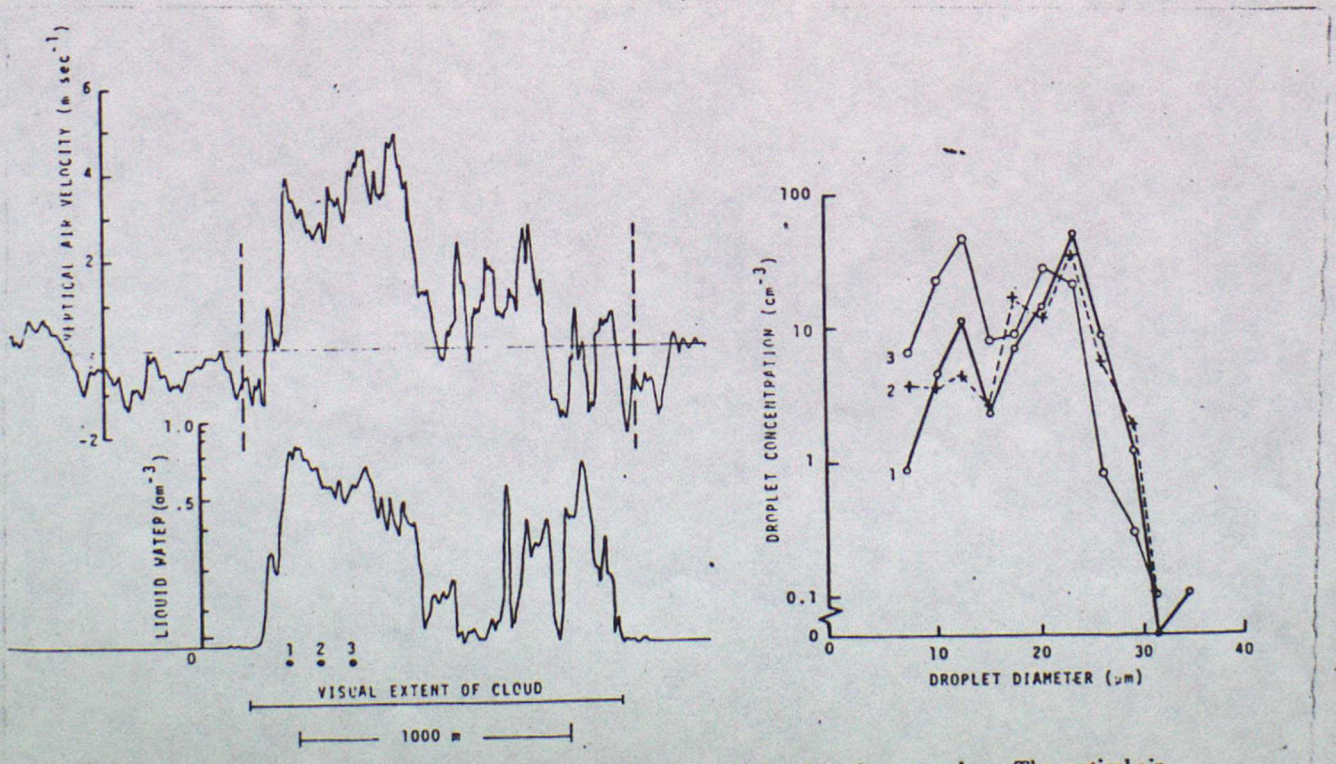

Bimodal droplet distributions within the body of a cloud nearly 1 km from its top or base. The vertical air velocity and liquid water content records are also shown.

FIGURE 1

(a) (b)

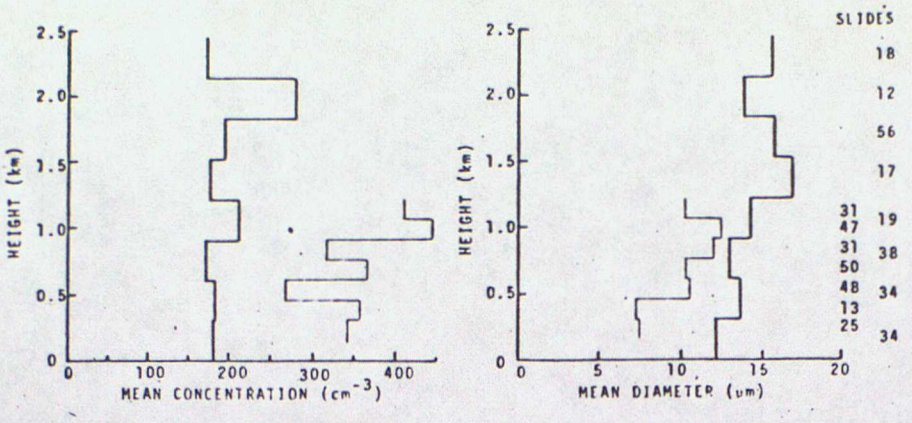

The variation with height of droplet concentration and mean droplet diameter averaged for all samples taken on each of two expeditions.

(c)

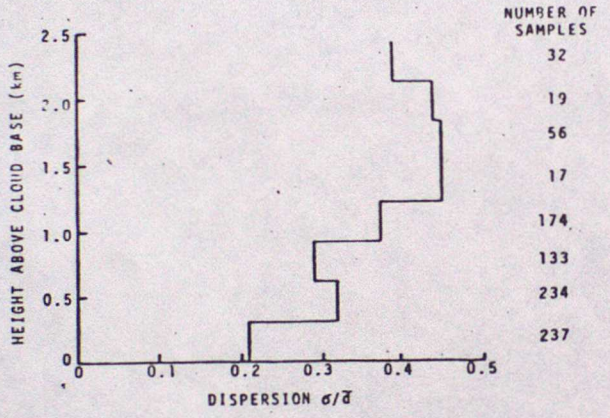

(d)

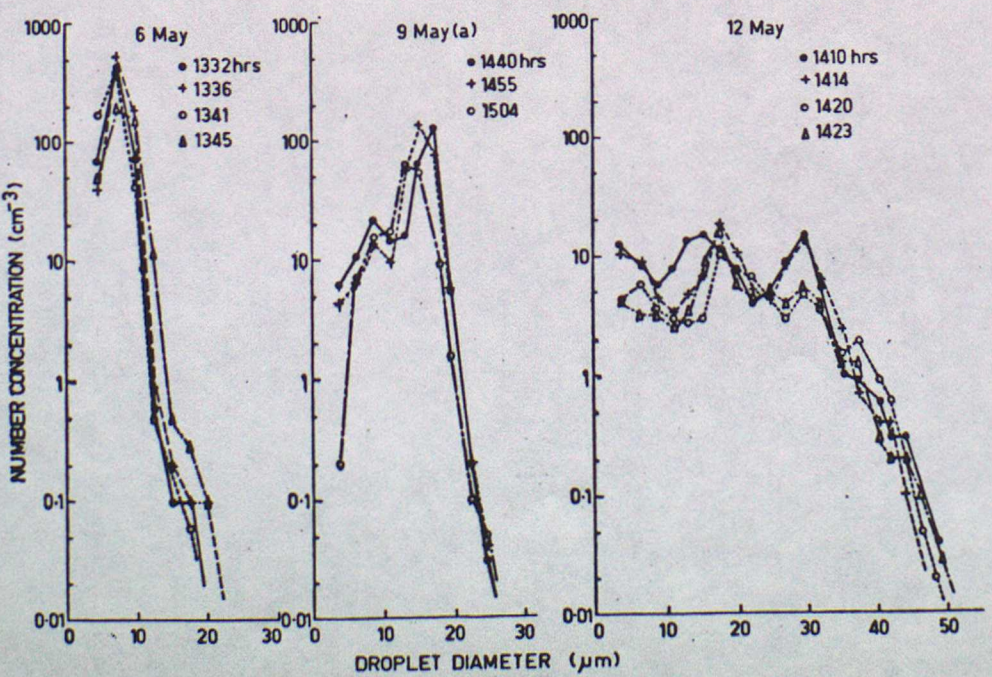

Droplet size distributions at different times at fixed levels for three clouds. The cloud sampled on 12 May produced fairly heavy rain.

FIGURE (2)

(a)

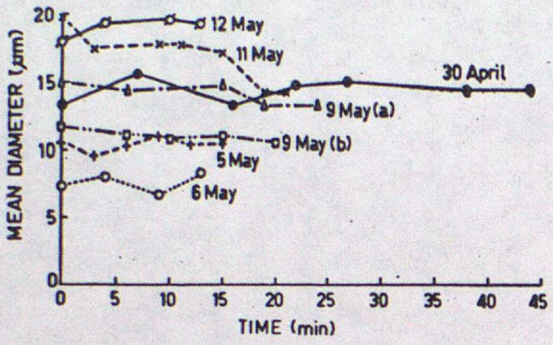

Changes in mean droplet diameter at fixed levels for seven clouds as the clouds aged.

(b)

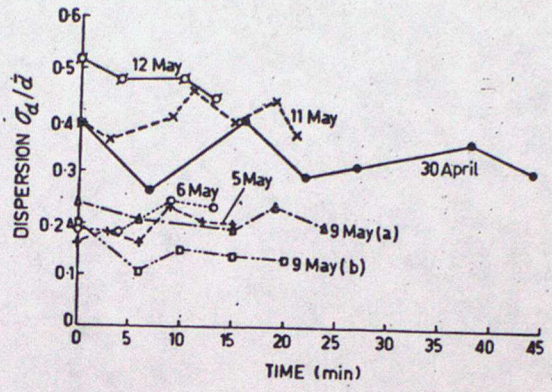

Changes in dispersion with time for the same clouds as those described by Fig. 3(a)

(c)

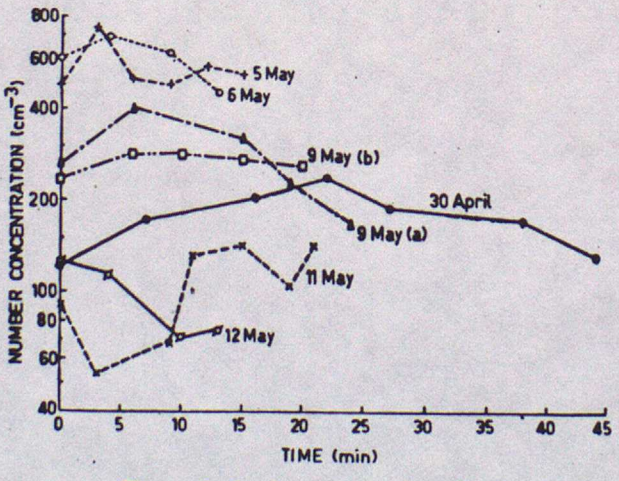

Changes in droplet concentration with time for the same clouds as those described by Fig. 3(a)

FIGURE (3)

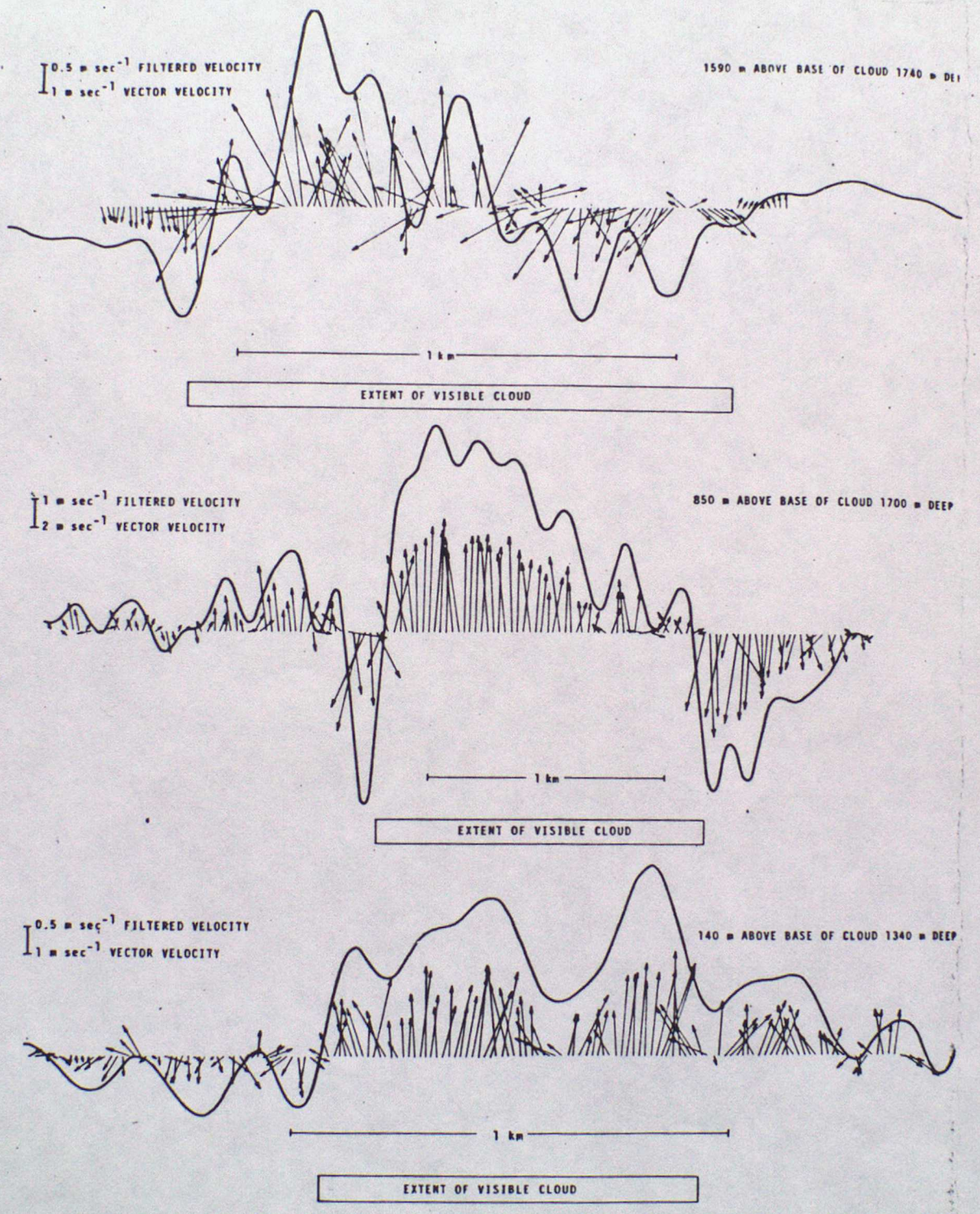

Vector air velocity at 0.2- or 0.4-sec intervals along the flight path through cumuli at different heights above cloud base. The vector is formed from the vertical air velocity and the gust velocity along the flight path; the lateral velocity was not measured. The smoothed vertical air velocity is shown by the full line. The bars represent the extent of the cloud at the traverse level.

FIGURE 4

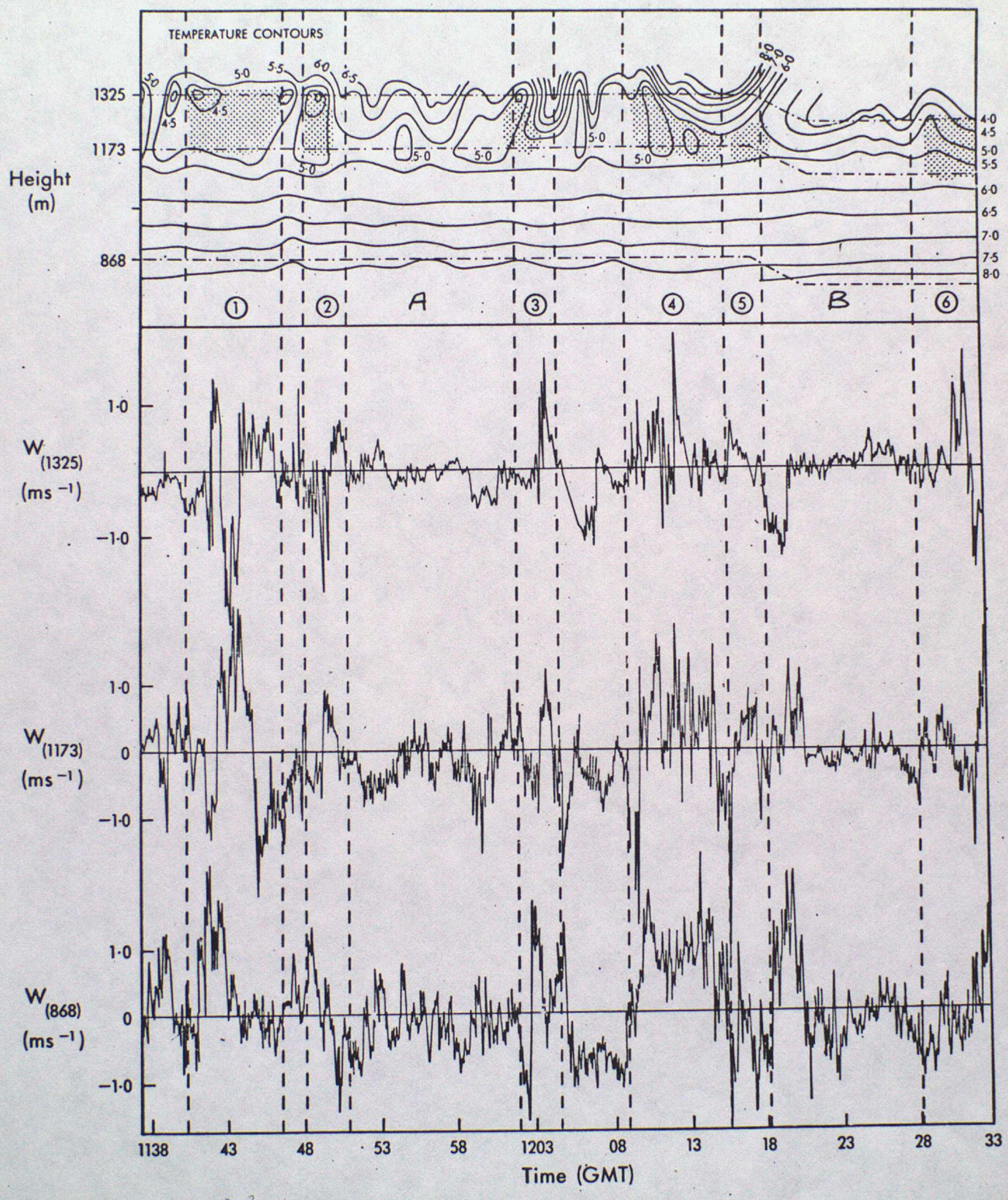
TEMPERATURE CONTOURS
Height (m)
1325
1173
868
4·0
4·5
5·0
5·5
6·0
6·5
7·0
7·5
8·0
① ② A ③ ④ ⑤ B ⑥
W(1325) (ms⁻¹)
W(1173) (ms⁻¹)
W(868) (ms⁻¹)
1·0
0
−1·0
1138
43
48
53
58
1203
08
13
18
23
28
33
Time (GMT)

Fig. 5

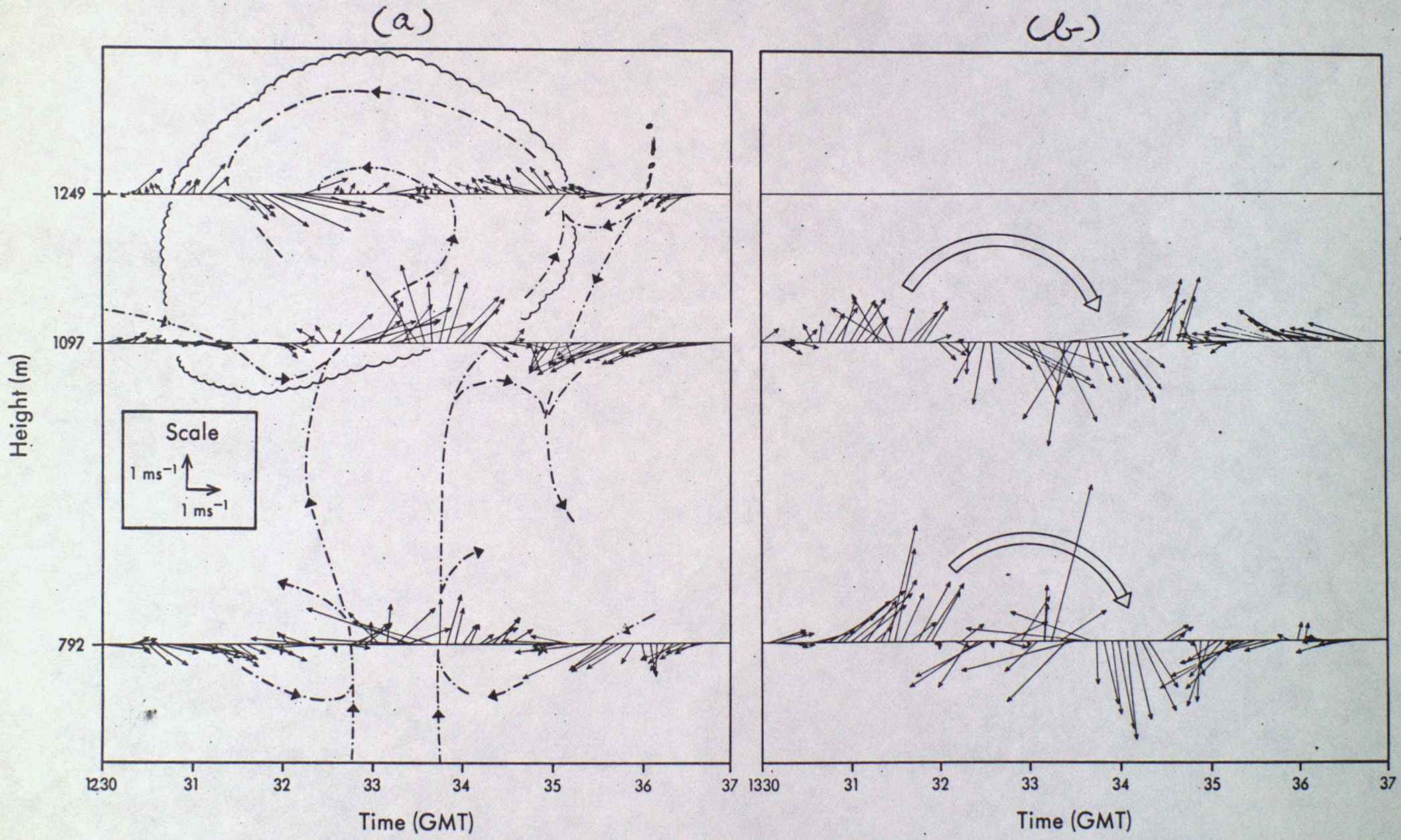
(a)
(b)
1249
1097
792
Height (m)
Scale
1 ms⁻¹
1 ms⁻¹
1230
31
32
33
34
35
36
37
1330
31
32
33
34
35
36
37
Time (GMT)
Time (GMT)

Fig. 6

(a)

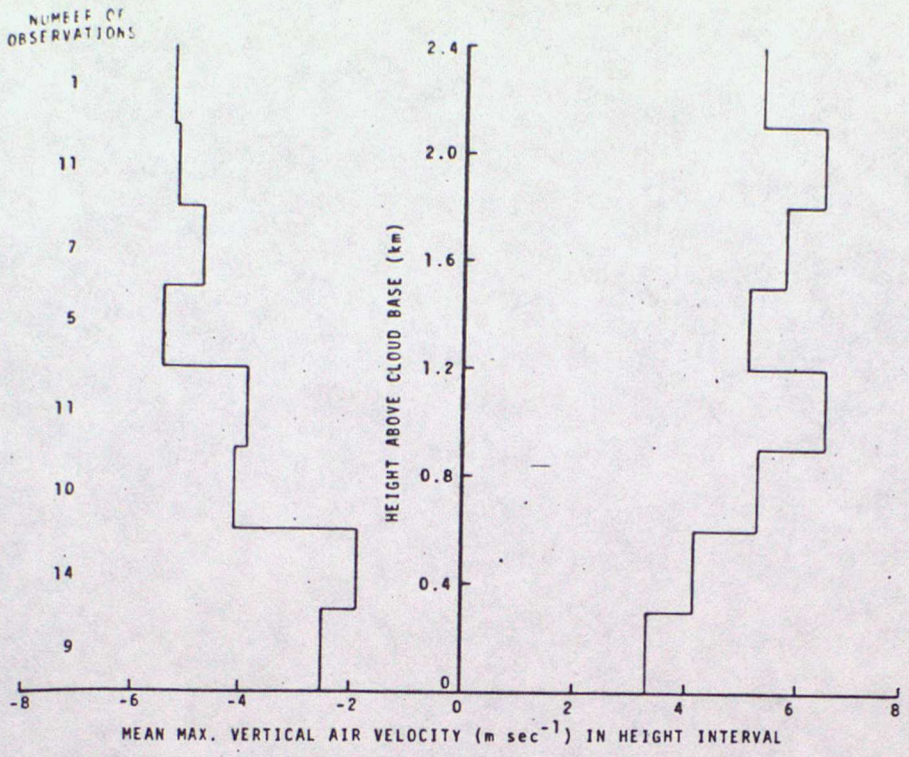

Variation of peak updraft and downdraft with height above cloud base. The 68 cloud traverses were stratified into 300 m height ranges. The standard deviation of the mean maximum vertical air velocity varied somewhat from one height interval to the next but averaged 1.6 m sec^{-1}.

(b)

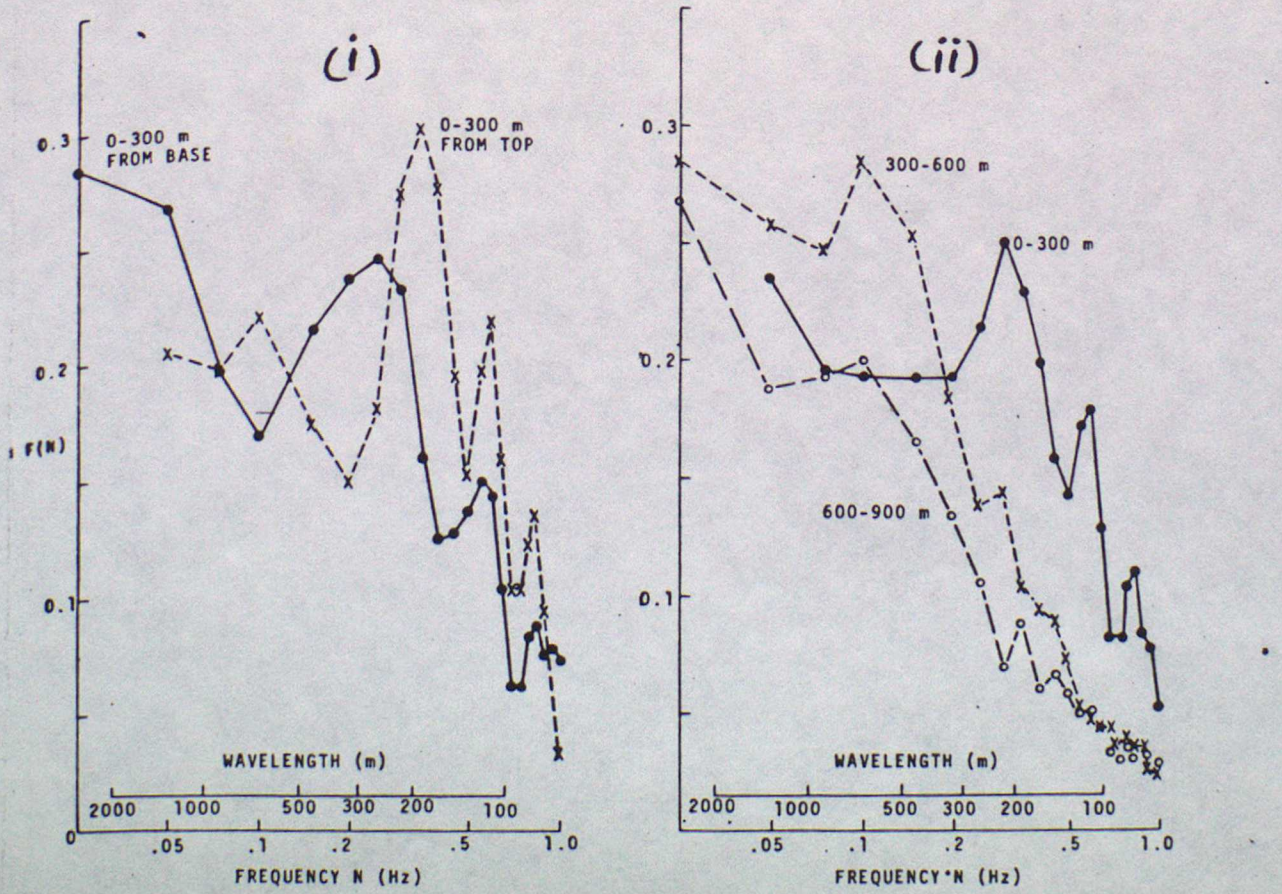

The variation of $NF(N)$ with frequency N for runs made at different distances from the cloud lower or upper boundary. The wavelength is obtained from the frequency on the basis of an aircraft speed of 65 m sec^{-1}.

FIGURE (7)

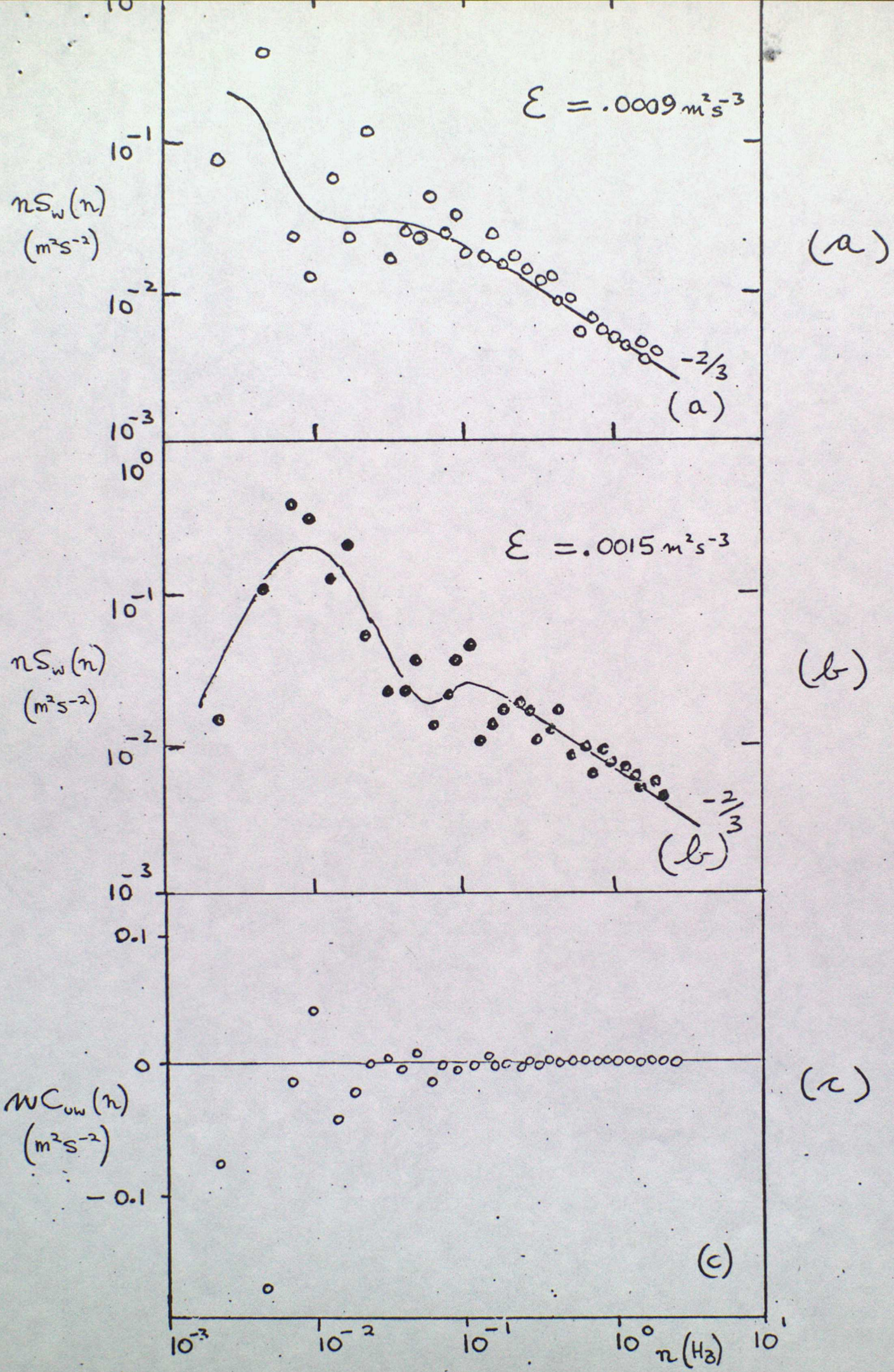
$\varepsilon = .0009\ m^2 s^{-3}$
$nS_w(n)$ $(m^2 s^{-2})$
10^{-1}
10^{-2}
10^{-3}
$-2/3$
(a)
$\varepsilon = .0015\ m^2 s^{-3}$
10^{0}
10^{-1}
10^{-2}
10^{-3}
$-\frac{2}{3}$
(b)
$nC_{uw}(n)$ $(m^2 s^{-2})$
0.1
0
-0.1
(c)
10^{-3}
10^{-2}
10^{-1}
10^{0}
10^{1}
$n(Hz)$

Fig. 8

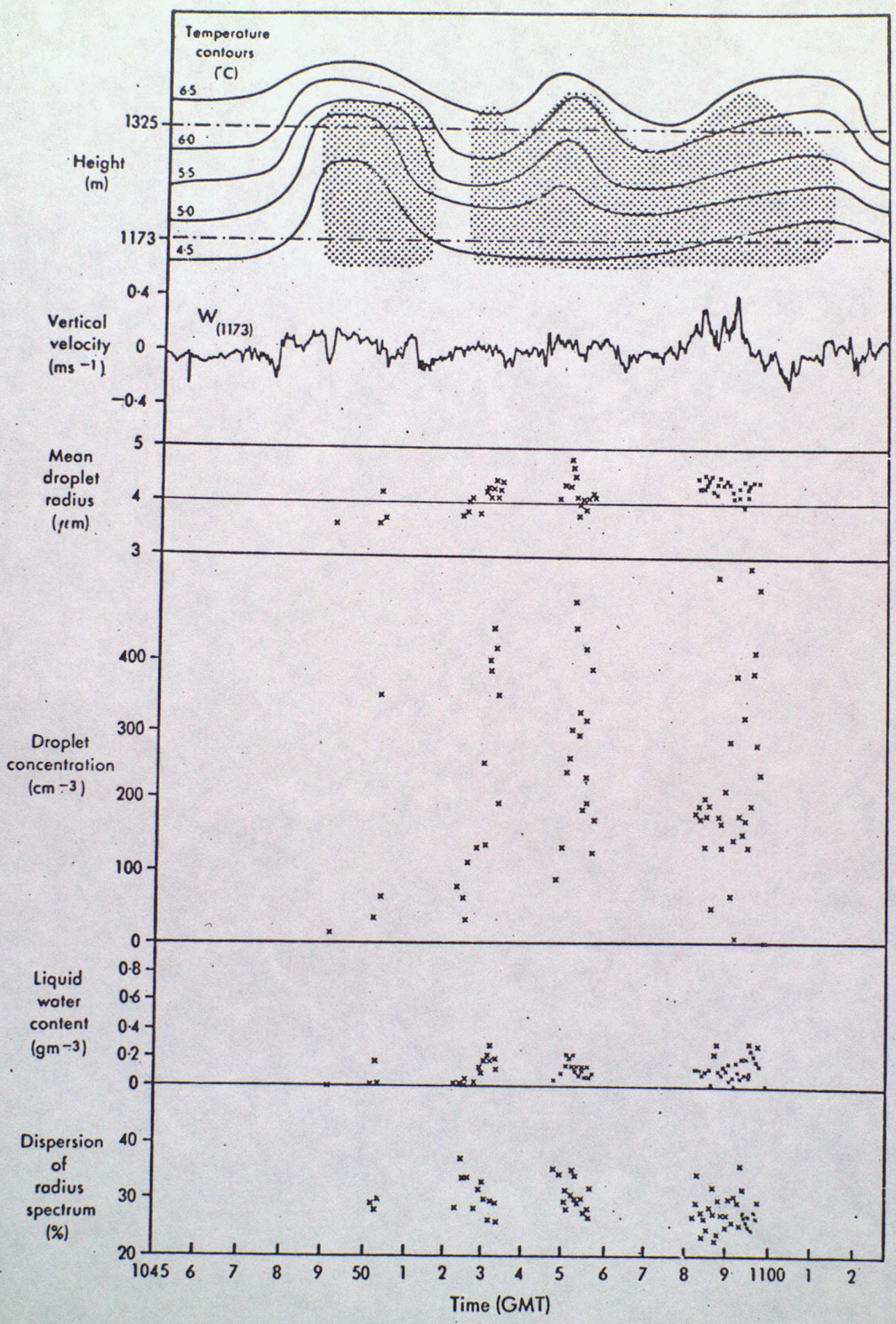
Temperature contours (°C)
6·5
6·0
5·5
5·0
4·5
1325
1173
Height (m)
0·4
0
−0·4
Vertical velocity (ms⁻¹)
W(1173)
5
4
3
Mean droplet radius (μm)
400
300
200
100
0
Droplet concentration (cm⁻³)
0·8
0·6
0·4
0·2
0
Liquid water content (gm⁻³)
40
30
20
Dispersion of radius spectrum (%)
1045 6 7 8 9 50 1 2 3 4 5 6 7 8 9 1100 1 2
Time (GMT)

FIGURE (9)

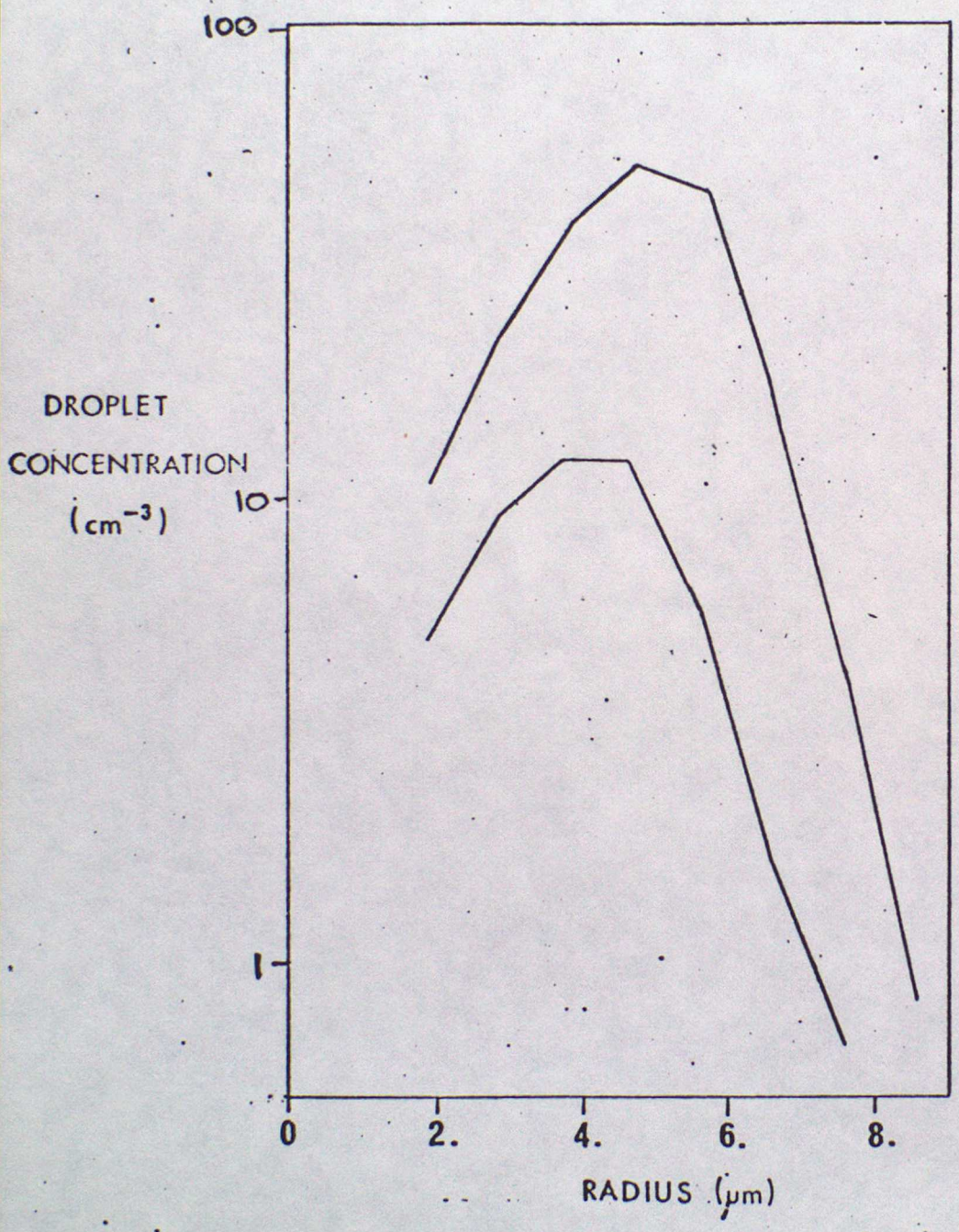

Fig. 10

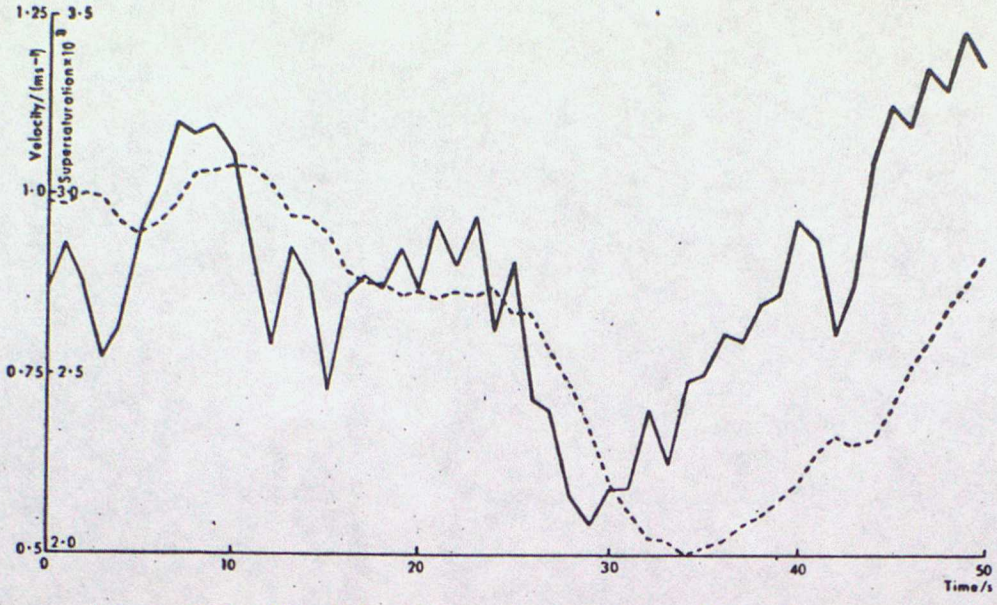

(a)

Diagram showing the variations with time of the velocity (solid line) and supersaturation (dashed line) of a typical parcel of air. The mean updraught is 1 m s^{-1} and the turbulent energy dissipation 0·01 $m^2 s^{-3}$.

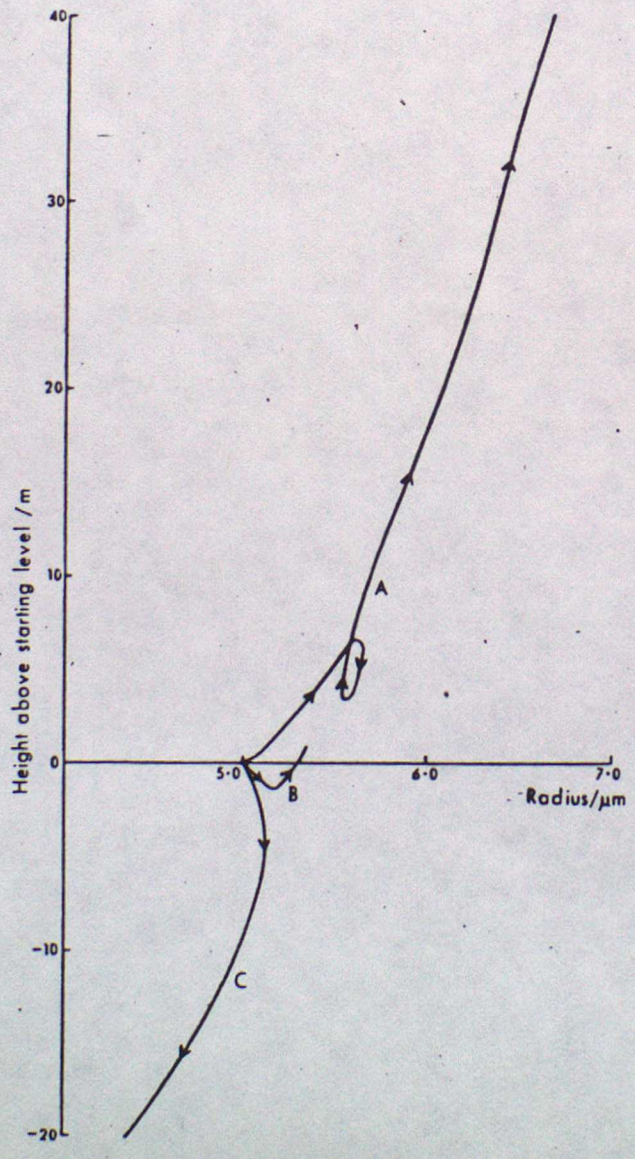

(b)

Diagram showing the variation of the radii of the droplets in three typical parcels of air with height above the starting level.

FIGURE (11)

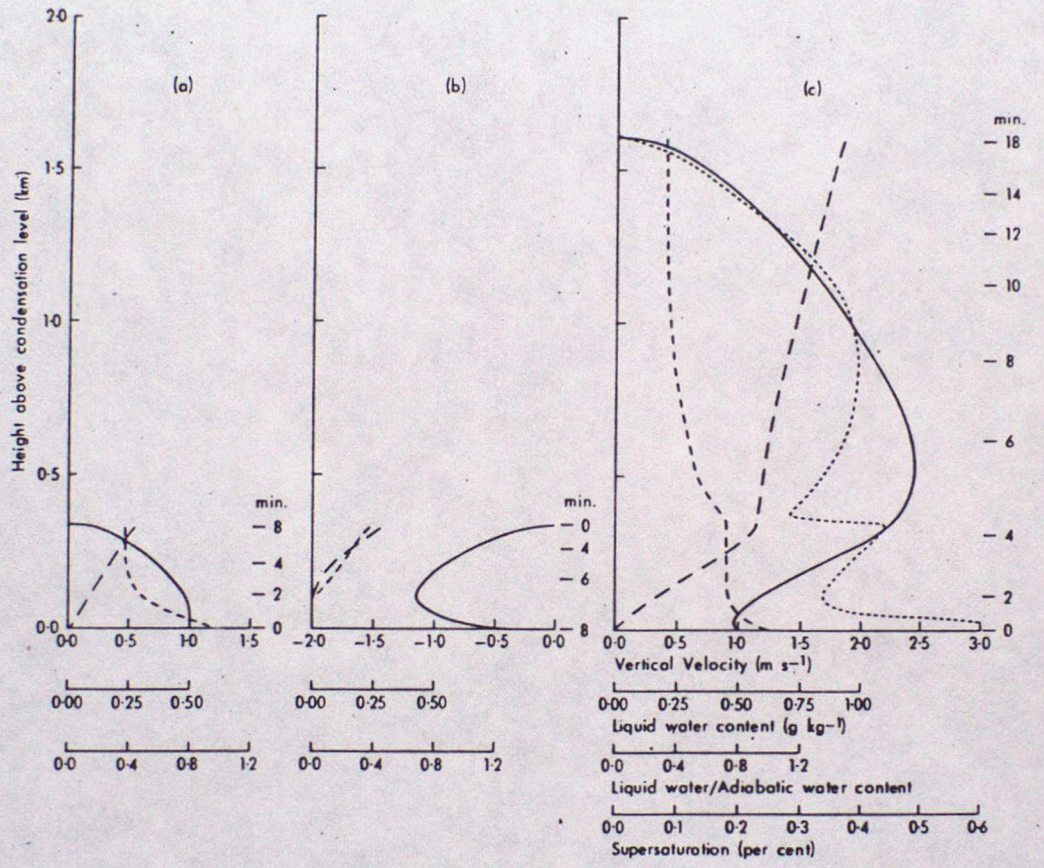

The development of successive thermals in a maritime cloud. Condensation level 900 mb, 10°C; $R_0 = 350$ m, $U_0 = 1$ m s^{-1}, $\Delta T_0 = 0{\cdot}1$°C, lapse rate $\alpha = 7$ deg C/km, environmental humidity $H' = 85$ per cent. The vertical velocity U, ————, liquid-water content W, — — — —, and the ratio of W to the adiabatic value W_a, – – – –, are plotted as functions of height.

(a) The ascent of the first thermal in clear air.

(b) The decay and descent of the first thermal.

(c) The ascent of a second thermal through the residue of the first.

The figures on the right of each diagram show the elapsed time (min) since the start of each stage. The progress of the supersaturation during the growth of the second thermal is shown ..... and was obtained for a nucleus population of 66 per mg of air.

FIGURE (12)

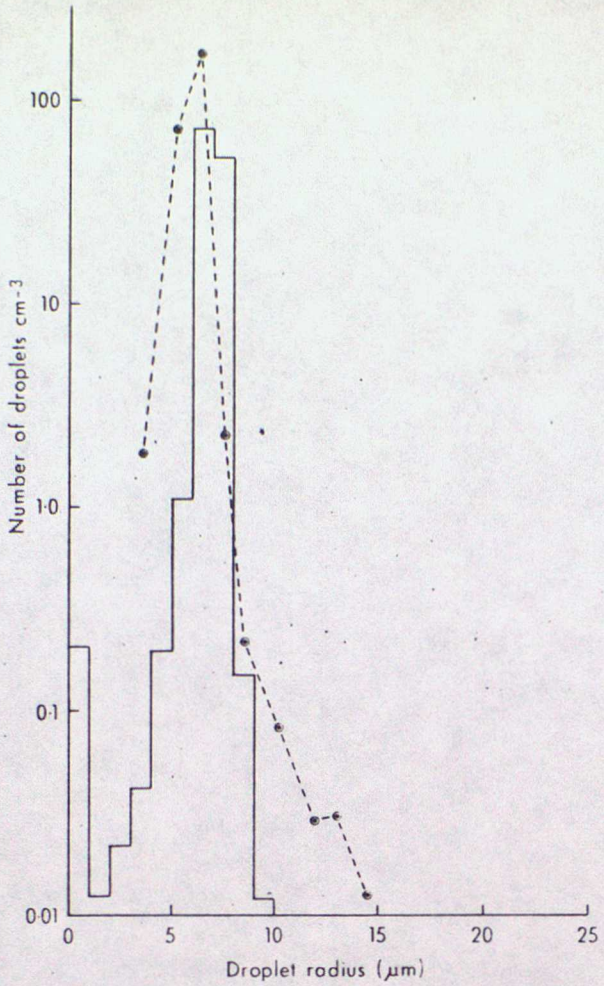

(a)

A comparison of a droplet spectrum predicted by the model after the ascent of a second thermal 150 m above the base of a maritime cloud now assumed to contain 130 nuclei/mg, with a spectrum (dashed line) measured by Warner at a similar height in a similar sized cloud where the total droplet concentration was 180 cm^{-3}.

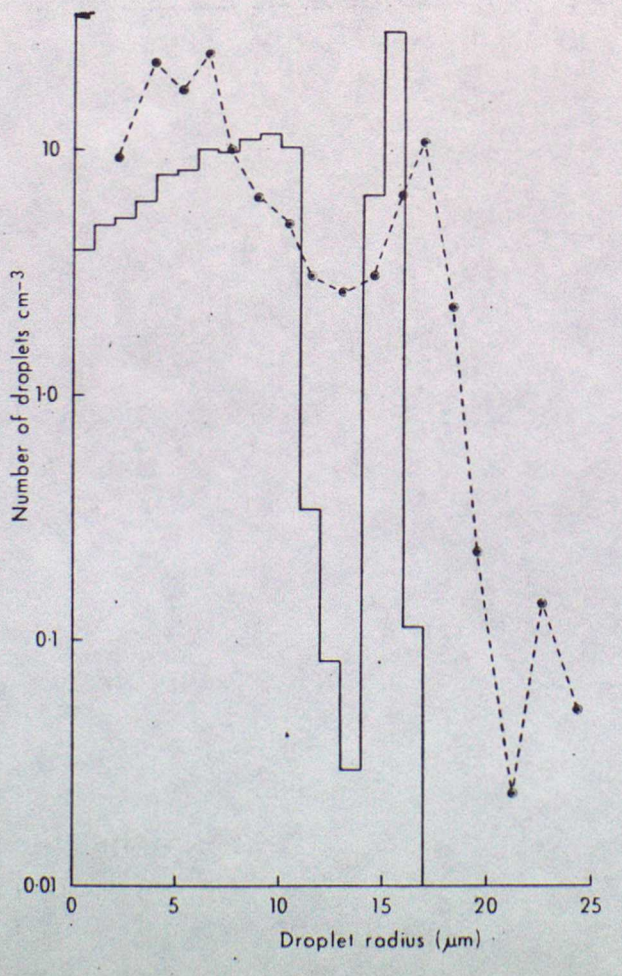

(b)

Comparison of the computed spectrum at 1·4 km above the condensation level in the maritime cloud of Fig. 1(c) and Fig. 4, with the mean of two spectra observed by Warner near the top of a cloud 1·4 km deep in which the droplet concentrations were 143 and 116 cm^{-3}.

FIGURE (13)

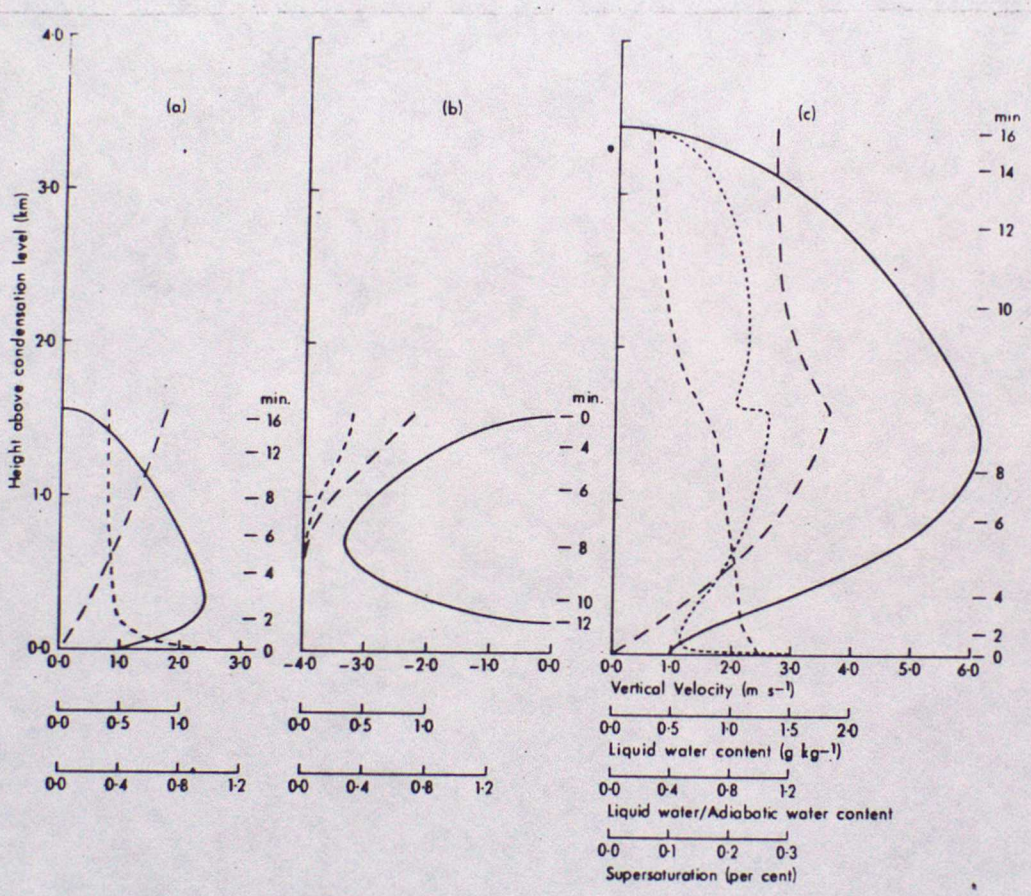

The development of a continental cloud on the same lines as for Fig. 1. $R_0 = 350$ m, $\Delta T_0 = 0{\cdot}6$°C, $U_0 = 1$ m s^{-1}, $\alpha = 7$ deg C/km, H′ = 85 per cent. Nucleus population = 530/mg.

FIGURE (14)

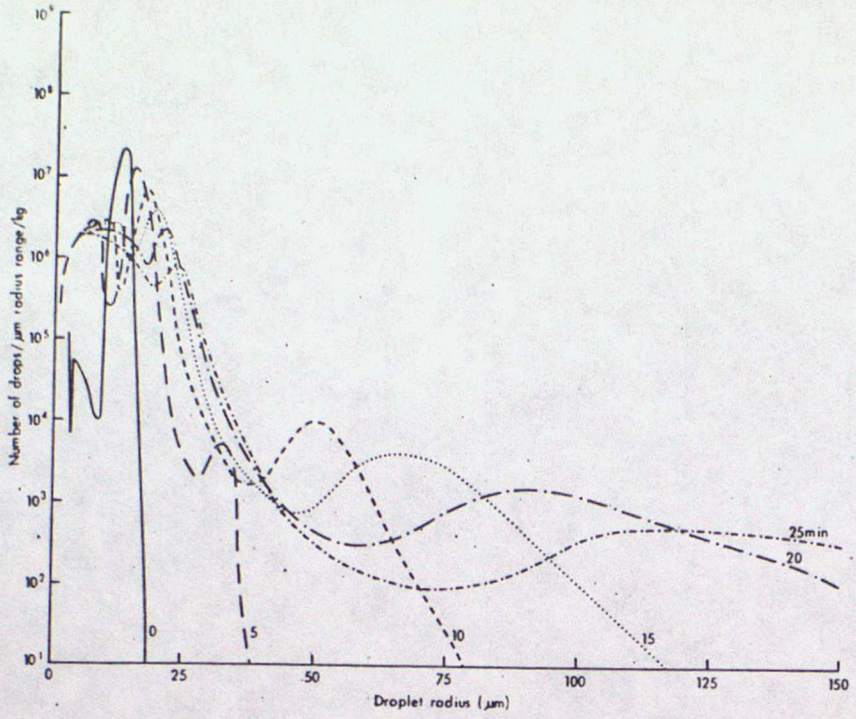

(a)

The development of a spectrum initially containing 65 droplets mg^{-1} by condensation and coalescence in the maritime cumulus of Mason and Jonas. The collection kernels of Fig. 1 were assumed together with an entrainment parameter of $1{\cdot}5 \times 10^{-3}\,s^{-1}$ and a supersaturation of 0·25%. Spectra are shown at 5-minute intervals.

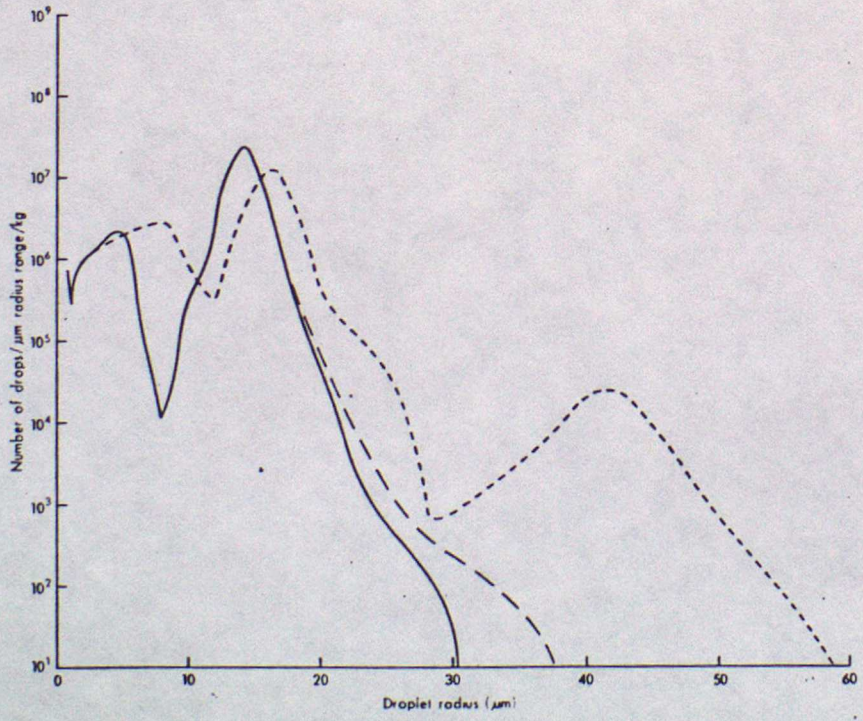

(b)

The development of an initial droplet spectrum (solid line) by coalescence when condensation is neglected (pecked line) and when it is included (dashed line). The development in both cases is over a 4-minute period and when condensation and entrainment are included. $\mu = 1{\cdot}5 \times 10^{-3}\,s^{-1}$ and $\sigma = 0{\cdot}25\%$.

FIGURE (15)

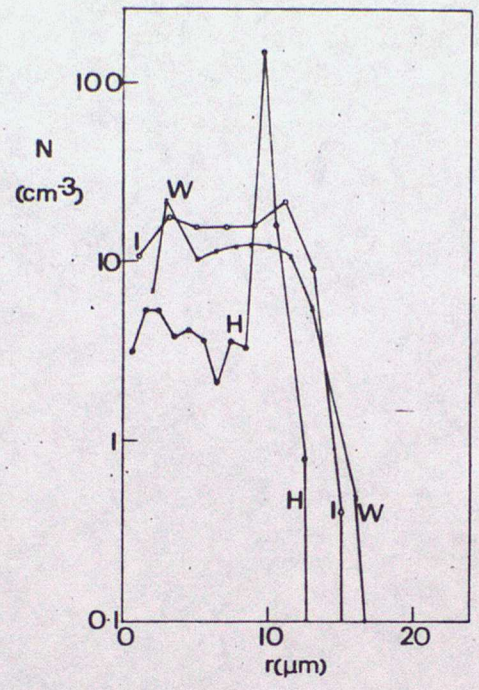

Droplet size distributions in cumulus: *W*, measured by Warner (1969a); *H*, calculated on the homogeneous model; *I*, calculated on the inhomogeneous model. $U = 1\,\mathrm{m\,s^{-1}}$, $1/\lambda_0 = 10\,\mathrm{s}$, $T(o) = 15°\mathrm{C}$, $N = 200\,\mathrm{cm^{-3}}$, $n = 6$, $\mu = 10^{-3}\,\mathrm{m^{-1}}$, $L = 0{\cdot}4\,\mathrm{g\,m^{-3}}$.

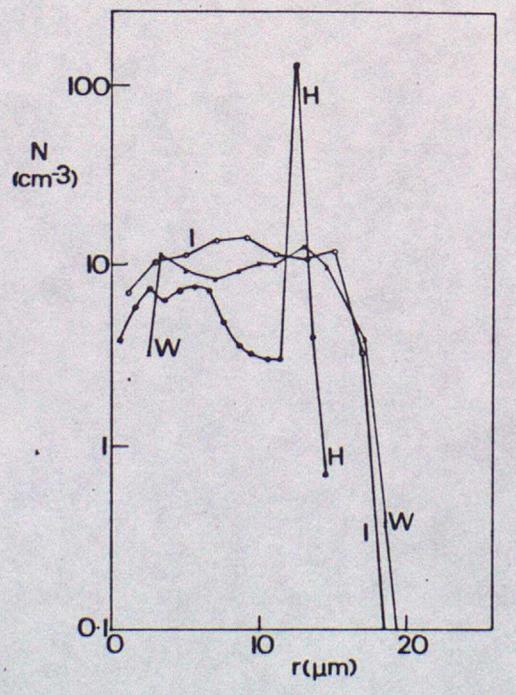

Droplet size distributions in cumulus: *W*, measured by Warner (1969a); *H*, calculated on the homogeneous model; *I*, calculated on the inhomogeneous model. $U = 1\,\mathrm{m\,s^{-1}}$, $1/\lambda_0 = 10\,\mathrm{s}$, $T(o) = 15°\mathrm{C}$, $N = 200\,\mathrm{cm^{-3}}$, $n = 6$, $\mu = 10^{-3}\,\mathrm{m^{-1}}$, $L = 0{\cdot}7\,\mathrm{g\,m^{-3}}$.

FIGURE (16)